Extracellular vesicles of stem cells to prevent BRONJ

Junna Watanabe, Kiyoshi Sakai, Yusuke Urata, Naoto Toyama, Eiji Nakamichi, Hideharu Hibi

Department of Oral and Maxillofacial Surgery, Nagoya University Graduate School of Medicine, Nagoya, Japan

Abstract word count: 274

Total word count (Abstract to Acknowledgments): 3,192

Total number of tables/figures: 5 figures

Number of references: 39

Keywords: Bisphosphonate-Associated Osteonecrosis of the Jaw, Mesenchymal Stem Cells, Extracellular Vesicles, Cellular Senescence, Zoledronic Acid, Wound Healing.

Abstract

Extracellular vesicles (EVs), several tens to hundreds of nanometers in size, are vesicles secreted by cells for intercellular communication. EVs released from mesenchymal stem cells (MSC-EVs) have the potential to treat multiple diseases. This study aimed to determine the effects of MSC-EVs on bisphosphonate-related osteonecrosis of the jaw (BRONJ), whose pathogenesis and treatment are not yet established.

To this end, zoledronic acid (ZOL) was administered to bone marrow cells and fibroblasts *in vitro*. *In vivo*, a BRONJ model was produced by administering ZOL to rats and extracting teeth. Each MSC-EV-treated and non-treated group was compared histologically and molecularly. *In vitro*, the non-treated group showed an increased number of β-galactosidase-positive cells and expression of senescence-associated genes *p21*, *pRB* and senescence-related inflammatory cytokines. Conversely, MSC-EVs administration decreased the number of senescent cells and expression levels of *p21*, *pRB* and inflammatory cytokines. *In vivo*, in the non-treated group, the socket was partially uncovered by the oral epithelium, leaving an exposed bone. Conversely, in the MSC-EV-treated group, the socket was healed. Besides, in the non-treated group, β-galactosidase-positive cells existed in the socket and co-localized with the CD90 and Periostin-positive cells. However,

there were few β-galactosidase-positive cells in the MSC-EV-treated group. Further, gene expression of stem cell markers *Bmi1* and *Hmga2* and the vascular endothelial marker *VEGF* was significantly increased in the MSC-EV-treated group, compared with that in the non-treated group. These results indicate that MSC-EVs prevent ZOL-induced senescence in stem cells, osteoblasts, and fibroblasts and reduce inflammatory cytokines. Furthermore, administration of MSC-EVs prevented senescence of cells involved in wound healing and the spread of chronic inflammation around senescent cells, thereby promoting angiogenesis and bone regeneration and preventing BRONJ.

Introduction

Zoledronic acid (ZOL), which is a bisphosphonate, is widely used in the treatment of bone metastasis of cancer and osteoporosis. However, some patients who receive bisphosphonates for a prolonged time period develop bisphosphonate-related osteonecrosis of the jaw, BRONJ. BRONJ is defined as exposed bone in the maxillofacial area that lasts for more than eight weeks, even without radiation therapy to the jaws (Ruggiero et al. 2014). The condition causes a marked decrease in patients' quality of life, such as pain, swelling, purulent discharge, and noxious-odor. Despite the severity of the disease, its pathophysiology remains unknown, and no appropriate treatment has been established. Recently, cell therapy using bone marrow-derived mesenchymal stem cells (MSCs) has been useful in treating many diseases (Uccelli et al. 2008). The use of MSCs in the treatment of BRONJ has been reported (Kikuiri et al. 2010; Li et al. 2013). MSCs control immune cells through secretion of various cytokines and secrete growth factors to promote regeneration of damaged tissues (Chamberlain et al. 2007). However, most transplanted MSCs do not survive long (Mummery et al. 2010; Ide et al. 2010). Transplantation of MSCs may have improved function in animal models due to paracrine effects (Mummery et al. 2010; Chen et al. 2008; Osugi et al. 2012; Matsubara et al. 2015; Ogata et al. 2015). However, one of the

purified factors in conditioned medium (CM) is extracellular vesicles (EVs), which are defined as lipid bilayer particles without nucleic release from cells. Cells release various types of membrane vesicles to the extracellular environment, called exosomes, which are formed during endocytosis, as well as microvesicles, which bud directly from the plasma membrane (Théry et al. 2018). These EVs play an essential role in intercellular communication by serving as a vehicle for cell-to-cell transfer of cytosolic proteins, lipids, and RNA (Valadi et al. 2007; Raposo and Stoorvogel 2013). In the paracrine effects of MSCs, EVs play an important role. Recent studies have shown that MSC-derived EVs (MSC-EVs) have therapeutic effects similar to MSCs transplantation (Phinney et al.2008; Bruno et al. 2009; Lai et al. 2011; Katsuda and Ochiya 2015). EVs not only maintain homeostasis but also influence the onset, progression, and pathophysiology of various diseases. The specific roles and mechanisms of action, as well as the clinical value of EVs in the diagnosis and treatment of several diseases, are a subject of extensive investigation. The possibility to treat patients with EV-based strategies requires further study.

We hypothesized that MSC-EVs could prevent BRONJ development by promoting wound healing. To test this hypothesis, a rat BRONJ model was created, and MSC-EVs were injected. Also, an *ex vivo* study, in which ZOL was administered to bone marrow cells and

fibroblasts, followed by MSC-EVs was performed. We studied the EVs effects and their target cells by histological and molecular biological evaluation.

Materials and Methods

MSCs Culture and EVs Isolation

Human bone marrow-derived MSCs were purchased from Lonza (PT-2501, Walkersville, MD) and cultured in Dulbecco's Modified Eagle's Medium (DMEM; Sigma-Aldrich, St. Louis, MO) supplemented with 10% fetal bovine serum (FBS; GE Healthcare Bioscience, Piscataway, NJ) at 37°C in 5% CO_2 until 90% confluent. MSC-EVs were extracted according to previous reports (Yokoi et al. 2017). Briefly, the cells were washed twice with phosphate-buffered saline (PBS), and the culture medium was replaced with Advanced DMEM (FBS free, Thermo Fisher Scientific). After incubation for 48 hours, the CM was collected. To thoroughly remove cellular debris, the CM was centrifuged at 2,000 x *g* for 10 minutes at 4°C, and the supernatant was filtered through a 0.22 μm filter (Merck Millipore, Billerica, MA). The CM was centrifuged at 100,000 x *g* using an ultracentrifuge (Optima L-100, Beckman Coulter, Inc. Brea, CA) and a swing rotor (SW Ti, Beckman Coulter) for 70 minutes

at 4°C and repeated four times. The pellets were washed with PBS, ultracentrifuged at 100,000 x g, and resuspended in PBS. The concentration of EVs was measured by the protein concentration of putative EVs fraction, using the Qubit Protein Assay Kit with Qubit 2.0 Fluorometer (Thermo Fisher Scientific, Waltham, MA). Specifically, 1 x 10^7 cells were initially seeded and cultured in 280 mL of medium. The EV-pellets were resuspended in 500 µL of PBS. The EVs concentration was approximately 60 µg/mL each time as measured by Qubit. We preferably using fresh EVs, but when they were stored, EVs were flash-frozen at -80°C.

Establishment of BRONJ Model

All experimental procedures involving animals were conducted following the National Institutes of Health Guidelines for the Care and Use of Laboratory Animals and were approved by the Nagoya University School of Medicine Animal Care and Use Committee (No. 30263, 31081).

Eighty-one 9-week-old female Wistar/ST rats (180-200 g) were obtained from Japan SLC, Inc. (Shizuoka, Japan). Rat BRONJ model was established according to previous reports (Sonis et al. 2009; Hokugo et al. 2010). For ZOL (Zoledronic acid, Sawai Pharmaceutical Co. Ltd.,

Osaka, Japan; 35 μg/kg), tail vein injection was repeated once a week for 3 weeks. Dexamethasone (DEX, Aspen Japan KK, Tokyo, Japan; 1 mg/kg) was intraperitoneally injected every day for 3 weeks. After general and local anesthesia, all three left maxillary molars were extracted with a dental explorer. The animals were randomly assigned to the following three groups: (1) control: without injecting ZOL and DEX, and without injecting anything else at the following day, only tooth extraction; (2) ZOL + PBS: in rats administered ZOL and DEX as described above, 0.5 mL of PBS was infused from the tail vein the day after tooth extraction; (3) ZOL + EVs: in rats administered ZOL and DEX, 30 μg/0.5 mL MSC-EVs were dissolved in PBS and injected into the tail vein the day after tooth extraction (Figure 2A).

Bone Marrow Cells, Fibroblasts, and Osteoclasts with ZOL

Rat bone marrow cells were collected from the femurs of 10 4-week-old male Wistar/ST rats (Zhang and Chan 2010), and human dermal fibroblasts were purchased from Lonza, and cultured in DMEM supplemented with 10% FBS. Rat osteoclasts were purchased from CosmoBio Co., Ltd. (Tokyo, Japan) and cultured in α-MEM with RANKL/M-CSF (CosmoBio Co., Ltd.), according to the instructions. Cancer cells (SAS, squamous carcinoma of the tongue) were obtained from Riken BRC (Tsukuba, Japan) and cultured in DMEM

supplemented with 10% FBS. Bone marrow cells, fibroblasts, osteoclasts, and cancer cells were cultured at 37°C in 5% CO_2, and then ZOL (Sawai Pharmaceutical; 100 μM) was administered and cells were cultured for another 24 hours. After that, MSC-EVs (10 μg/mL) or PBS were added to the cultured cells. The control group did not receive ZOL, but the DMEM was replaced.

Analysis of MSC-EVs

The isolated MSC-EVs were visualized using a transmission electron microscope (JEM-1400PLUS, JEOL, Tokyo, Japan) by negative staining. To determine the particle size distribution of MSC-EVs, a particle size measurement system (ELSZ-2, Otsuka Electronics Co., Ltd., Osaka, Japan) was used, according to the manufacturer's protocol. The exosomes markers (CD63, CD9, and CD81) were detected by western blotting. The purified EVs were fluorescently labeled with PKH26 Red Fluorescent Labeling Kit (Sigma-Aldrich; 4 μM) using Amicon Ultra-0.5mL centrifugal filter-100K (Merck Millipore), according to the manufacturer's instructions, to assess their uptake by rat bone marrow cells. PKH26-labeled EVs were administered into the culture medium of rat bone marrow cells, and 18 hours later, cells were

counterstained with Hoechst33342 (Thermo Fisher Scientific). Cells images were observed through a fluorescence microscope (BZ9000; Keyence Co., Osaka, Japan).

***In Vivo*: Effects of EVs in the Rat BRONJ Model**

Rats were deeply anesthetized before sacrifice. The upper jaw was removed for preparation of histological specimens (paraffin-embedded and frozen specimens), X-ray computed microtomography (μCT) imaging, and qRT-PCR. μCT was taken prior to hematoxylin and eosin (H&E) staining with paraffin-embedded specimens at 3, 7, 14 days, and 8 weeks after administration. Fluorescence immunohistochemical staining (β-galactosidase, CD90, Periostin, VEGFR2 and CD31) and Tartrate-Resistant Acid Phosphatase (TRAP) staining with frozen samples were performed 14 days after administration. Gene expression associated with cellular senescence, inflammation, and self-renewal was assessed by qRT-PCR (Appendix Table: *p21*, *pRB*, *IL-6*, *IL-8*, *MMP1*, *MMP3*, *VEGF*, *Bmi1* and *Hgma2*) 14 days after administration. The respective fold changes were calculated with respect to the control. Detailed information is provided in Appendix Materials and Methods. All experiments of 14 days were n = 6 per group. The experiments of 3 days, 7 days, and 8 weeks were n = 3 per group.

***Ex Vivo*: Effects of EVs on rat Bone Marrow Cells, Fibroblasts, Osteoclasts, and Cancer Cells with ZOL**

ZOL was administered as described above, to perform the following evaluations. Cell proliferation was assessed with wound healing (Cell Biolabs, Inc. San Diego, CA) and WST-8 (Cell Counting Kit-8, DOJINDO, Kumamoto, Japan) at 48 hours after MSC-EVs administration. β-galactosidase (SPiDER-βGal, DOJINDO)-positive cells were detected at 24 and 48 hours. The total RNA was extracted from the cells with TRIzol reagent (Thermo Fisher Scientific), according to the manufacturer's protocol (noted Appendix Materials and Methods), followed by qRT-PCR (Appendix Table: *p21, pRB, IL-6, IL-8, MMP1* and *MMP3*) at 48 hours. Additionally, apoptotic osteoclasts were counted using TUNEL (In Situ Cell Death Detection Kit, Roche, Basel, Switzerland) at 48 hours, and cancer cells were counted using WST-8 at 48 hours and wound healing assay at 24 hours. All *ex vivo* experiments were n = 6 per group.

Statistical Analysis

Results are presented as mean ± SEM of at least three independent experiments. All actual data values are given in the Appendix.

Statistical analysis was performed using SPSS for Windows, version 19.0 (IBM, New York, USA). An unpaired two-tailed Student's t-test was applied when comparing two groups. To analyze three or more independent groups, we used a one-way analysis of variance (ANOVA), followed by Tukey's post hoc test. Differences were considered statistically significant when $p < 0.05$.

Results

Characterization of EVs and Confirmation of Uptake into Cells

Morphology of MSC-EVs and the presence of lipid bilayer membranes were confirmed by transmission electron microscopy (Fig. 1A). The particle size measurement also confirmed the size and its distribution. The MSC-EVs contained several sizes with a peak at 100 nm (Fig. 1B). Moreover, protein markers CD63, CD9, and CD81 specifically present on the surface of exosomes were detected by western blotting. In the extracted EVs, presence of α-tubulin, which is a cell component, was not observed (Fig. 1C). Further, we confirmed that the EVs were taken into the cell cytoplasm when rat bone marrow cells incorporated EVs fluorescently-labeled with PKH26 (Fig. 1D).

Establishment of BRONJ Model and Effect of MSC-EVs on Wound Healing

The establishment of the rat BRONJ model was confirmed by the fact that the socket was not covered with mucosa, and the alveolar bone was exposed after 8 weeks of tooth extraction (Fig. 2B). Two weeks after tooth extraction, the removed maxillary specimens revealed that there was no covering of the gum tissue in the tooth extraction cavity and exposed alveolar bone in the ZOL + PBS group. However, in the ZOL + EVs group, the extraction socket was covered with soft tissue (Fig. 2B and 2E). When comparing each sample by μCT, there was less hard tissue in the extraction socket of the ZOL + PBS group than in the ZOL + EVs group (Fig. 2C and 2F). H&E staining confirmed the continuity of the epithelium in the ZOL+EVs group at 2 and 8 weeks (Fig. 2D).

Effects of MSC-EVs on Cellular Senescence

As a result of the administration of 100 μM ZOL to rat bone marrow cells and fibroblasts, interestingly, a flattening of cell morphology and a significant increase in the number of β-galactosidase-positive cells specific for senescent cells were observed. However, β-galactosidase-positive cells were significantly reduced in the ZOL + EVs group (Fig. 3A, 3B

and 3C). The expression of *p21* and *pRB*, which are involved in cellular senescence, were upregulated in the ZOL + PBS group but not in the ZOL + EVs group (Fig. 3D). Additionally, *IL-6*, *IL-8*, *MMP1,* and *MMP3*, were elevated in the ZOL + PBS group but not in the ZOL + EVs group (Fig. 3D). Migration of bone marrow cells and fibroblasts were assessed by wound healing assay at 24 and 48 hours after administration of EVs. As time went by, the scratched area shrank in the control and ZOL + EVs groups but not in the ZOL + PBS group (Fig. 3E and 3F). In the same way, proliferation capacity of bone marrow cells and fibroblasts was evaluated by WST-8. Although cell growth in the ZOL + PBS group was significantly reduced compared to the control group, the addition of EVs resulted in restoration of cell proliferation (Fig. 3G).

Target Cells of MSC-EVs

The presence of senescent cells was also observed in rat tissues, according to immunohistochemical staining. First, β-galactosidase-positive cells were present in the extraction socket of the ZOL + PBS group, but rarely in the control and ZOL + EVs groups (Fig. 4A, 4B and 4E). At the same time, we observed double staining of β-galactosidase with CD90 or Periostin only in the ZOL + PBS group (Fig. 4A and 4B). Next, almost no VEGFR2

and CD31 was observed in the ZOL + PBS group, as a difference with ZOL + EVs and the control groups (Fig. 4C and 4D). Furthermore, gene expression in rat maxillary bone tissue was evaluated. Similar results to those obtained *in vitro* were also shown in rat models. The expression levels of *p21* and *pRB* were elevated in the ZOL + PBS group but not in the PBS + EVs group (Fig. 4D). *IL-6*, *IL-8*, *MMP1,* and *MMP3* were elevated in the ZOL + PBS group but not in the ZOL + EVs group (Fig. 4D). Administration of MSC-EVs to the rat BRONJ model increased *Bmi1* and *Hmga2* gene expression, which are specifically expressed in stem cells (Fig. 4G).

Effects of EVs on Osteoclasts and Cancer Cells

Rat osteoclasts were cultured with ZOL the osteoclasts showed apoptosis. Furthermore, the number of apoptotic osteoclasts did not change significantly after EVs administration (Fig. 5A and 5B). *In vivo* detection of osteoclasts by TRAP staining showed less osteoclast staining in the ZOL + PBS and ZOL + EVs groups than in the control group and no increase in the stained area in the ZOL + EVs group (Fig. 5C). Additionally, as a result of the administration of ZOL and EVs to cancer cells, no marked proliferation of cancer cells was observed (Fig. 5D and Appendix Fig. 3).

Discussion

In this study, we reported that MSC-EVs prevented BRONJ via suppressing ZOL-mediated osteoblast, stem cell, and fibroblast aging and promoted wound healing. Specifically, *in vitro* ZOL-treated bone marrow cells and fibroblasts showed flattened cell morphology, decreased cell proliferation, increased expression of β-galactosidase, upregulated expression of senescence-associated genes *p21*, *pRB,* and senescence-related pro-inflammatory cytokines, and exhibited typical features of cellular senescence. However, when MSC-EVs were administered, cellular senescence was halted, remaining similar to the control group. *In vivo,* MSC-EVs prevented ulceration and bone exposure and promoted both angiogenesis and bone regeneration.

Bisphosphonates are effective due to their ability to strongly bind to bone mineral and to suppress osteoclast function (Russell et al. 2008). Other effects have been reported, such as the promotion of osteoblast differentiation (Fujita et al. 2011), inhibition of osteocyte apoptosis (Plotkin et al. 2006), and endothelial cell angiogenesis (Colombel et al. 2002).

Bisphosphonate pamidronate induced senescence in human keratinocytes (Kim et al. 2011). Here, for the first time, we demonstrated cellular senescence by zoledronate in the BRONJ model. We believe that the concentration of bisphosphonates that was administered caused apoptosis in osteoclasts but caused cellular senescence in the other cell types. Similar to apoptosis, when healthy cells suffer irreparable DNA damage due to various causes (Campisi and Fagagna 2007), cellular senescence acts as a biodefense mechanism preventing the growth of damaged and potentially dangerous cells. Senescent cells secrete various factors, such as cytokines and chemokines, which have inflammatory and carcinogenic effects, and extracellular matrix-degrading enzymes causing a phenomenon called "senescence-associated secretory phenotype (SASP)" (Rodier and Campisi 2011). SASP factors are known to act in an autocrine manner and enhance their cellular senescence (Acosta et al. 2008). It was also evidenced that paracrine signaling acts on surrounding cells (Acosta et al. 2013). The secreted SASP may provide the surrounding tissue with an unfavorable microenvironment that promotes inflammation and carcinogenesis. In this study, we also confirmed the presence of IL-6, IL-8, MMP1, and MMP3 in SASP after ZOL administration, which suggests that this is one of the mechanisms causing chronic inflammation and delayed wound healing in BRONJ. As a result of suppression of cell

senescence by EVs administration, secretion of SASP factors was reduced, and chronic inflammatory signals were not transmitted to surrounding cells, which may have led to healthy wound healing.

Bmi1 and *Hmga2* are known as genes that promote stem cell self-renewal by negatively regulating the expression of tumor suppressors of $p16^{INK4a}$/*pRB* and *p53*/*p21* pathways (Liu et al. 2009; Yamazaki et al. 2013). Further, CD90, a marker for MSCs, and periostin, expressed in osteoblasts, are essential regulators of the cell cycle (Khurana et al. 2013). Observation of the expression of *Bmi1* and *Hgma2* and localization of CD90 and periostin suggest aged cells and EVs target cells.

The administration of bisphosphonates to patients with bone metastases delays and reduces the incidence of skeletal-related events, such as pathological fractures, spinal cord compression, radiotherapy, surgery, and hypercalcemia (Urbanowitz et al. 2003). Therefore, doctors choose to give bisphosphonates to patients. It is necessary to prevent BRONJ while using ZOL. To accomplish this, a drug that does not block osteoclast apoptosis and is not carcinogenic is needed. In this study, we confirmed that MSC-EVs did not suppress

osteoclast apoptosis (Fig. 5A and 5B) and did not promote cancer cell growth (Fig. 5C and Appendix Fig. 4). Recently, the anti-apoptotic effect of MSC-EVs in endoplasmic reticulum stress has been reported (Liao et al. 2019), but it was considered that the effect of MSC-EVs may differ from cell to cell and that the effect of EVs in cells affected by drugs may differ. Therefore, the EVs do not counteract the effect of ZOL, which inhibits bone resorption, and it is expected to prevent BRONJ by suppressing the senescent cells surrounding osteoclasts, including stem cells. Given our results, we believe that MSC-EVs can serve as drugs that forestall BRONJ. However, the disadvantages of using MSC-EVs are that they require much work to extract after mass cultivation of MSCs and that, ideally, EVs are used fresh, as certain storage conditions may affect their stability and function. Therapeutic dose and frequency should be further investigated. Although detailed mechanisms remain unknown and warrant further study, clinical trials have already proven that EV-based therapies are safe and effective (Kordelas et al. 2014). Using MSC-EVs instead of directly transplanting the cells may lead to development of therapies that minimize the risks of side effects associated with cell-based regenerative medicine (for example, pulmonary embolism after transplantation). As an intercellular communication tool that stably transports the material contained in EVs, it can be expected to be utilized for the drug delivery to the treatment target cell. Our results

also anticipate that the use of EVs derived from MSCs may lead to the development of less invasive and more reliable therapies while maintaining the patient's quality of life.

Author Contributions

J. Watanabe, contributed to conception, design, data acquisition, and interpretation, performed statistical analyses, drafted the manuscript; K. Sakai, contributed to conception, design, data interpretation, drafted and critically revised the manuscript; Y. Urata, contributed to data acquisition and interpretation, critically revised the manuscript; N. Toyama, contributed to data acquisition, analysis and interpretation, performed statistical analyses, critically revised the manuscript; E. Nakamichi, contributed to data acquisition and interpretation, drafted the manuscript; H. Hibi, contributed to design and critically revised the manuscript. All authors gave their final approval and agreed to be accountable for all aspects of the work.

Acknowledgments

We are grateful to Kazuto Okabe, Takeshi Tsuruta, Yukiko Sugimura-Wakayama, and Kohei Sakaguchi from the Department of Oral and Maxillofacial Surgery, Nagoya University Graduate School of Medicine, for their comments and support of this study. We also thank Yoshimitsu Sakaguchi and Hajime Ito from Molecule & Material Synthesis Platform, Nagoya University, and Koji Itakura, Ryoko Sakamoto, Ikuyo Mizuguchi, and Eri Yorifuji from Division for Medical Research Engineering, Nagoya University Graduate School of Medicine for technical instruction for technical support and assistance. We thank the Division of Experimental Animals and Medical Research Engineering, Nagoya University Graduate School of Medicine, for rat housing. This work was supported by Grant-in-Aid for Young Scientists (B) from the Ministry of Education, Culture, Sports, Science and Technology of Japan. We declare no potential conflicts of interest with respect to the authorship and/or publication of this article.

References

1 Acosta JC, Banito A, Wuestefeld T, Georgilis A, Janich P, Morton JP, Athineos D, Kang TW,
2 Lasitschka F, Andrulis M, et al. 2013. A complex secretory program orchestrated by the
3 inflammasome controls paracrine senescence. Nat Cell Biol. 15(8):978-990.
4 Acosta JC, O'Loghlen A, Banito A, Guijarro M V., Augert A, Raguz S, Fumagalli M, Da Costa
5 M, Brown C, Popov N, et al. 2008. Chemokine signaling via the CXCR2 receptor
6 reinforces senescence. Cell. 133(6):1006-1018.
7 Bruno S, Grange C, Deregibus MC, Calogero RA, Saviozzi S, Collino F, Morando L, Busca A,
8 Falda M, Bussolati B, et al. 2009. Mesenchymal stem cell-derived microvesicles protect
9 against acute tubular injury. J Am Soc Nephrol. 20(5):1053-1067
10 Campisi J, d'Adda di Fagagna F. 2007. Cellular senescence: when bad things happen to
11 good cells. Nat Rev Mol Cell Biol. 8(9):729-740.
12 Chamberlain G, Fox J, Ashton B, Middleton J. 2007. Concise review: mesenchymal stem
13 cells: their phenotype, differentiation capacity, immunological features, and potential for
14 homing. Stem Cells. 25(11):2739-2749.
15 Chen L, Tredget EE, Wu PYG, Wu Y, Wu Y. 2008. Paracrine factors of mesenchymal stem
16 cells recruit macrophages and endothelial lineage cells and enhance wound healing.
17 PLoS One. 3(4):e1886.

Fournier P, Boissier S, Filleur S, Guglielmi J, Cabon F, Colombel M, Clézardin P. 2002. Bisphosphonates inhibits angiogenesis in vitro and testosterone-stimulated vascular regrowth in the ventral prostate in castrared rats. Cancer Res. 62(22):6538-6544.

Fujita H, Kurokawa K, Ogino T, Ono M, Yamamoto M, Oka T, Nakanishi T, Kobayashi N, Tanaka N, Ogawa T, et al. 2011. Effect of risedronate on osteoblast differentiation, expression of receptor activator of NF-κB ligand and apoptosis in mesenchymal stem cells. Basic Clin Pharmacol Toxicol. 109(2):78-84.

Hokugo A, Christensen R, Chung EM, Sung EC, Felsenfeld AL, Sayre JW, Garrett N, Adams JS, Nishimura I. 2010. Increased prevalence of bisphosphonate-related osteonecrosis of the jaw with vitamin D deficiency in rats. J Bone Miner Res. 25(6):1337-1349

Ide C, Nakai Y, Nakano N, Seo TB, Yamada Y, Endo K, Noda T, Saito F, Suzuki Y, Fukushima M, Nakatani T. 2010. Bone marrow stromal cell transplantation for treatment of sub-acute spinal cord injury in the rat. Brain Res. 1332:32-47.

Karnoub AE, Dash AB, Vo AP, Sullivan A, Brooks MW, Bell GW, Richardson AL, Polyak K, Tubo R, Weinberg RA. 2007. Mesenchymal stem cells within tumour stroma promote breast cancer metastasis. Nature. 449(7162):557-563.

1 Katsuda T, Ochiya T. 2015. Molecular signatures of mesenchymal stem cell-derived
2 extracellular vesicle-mediated tissue repair. Stem Cell Res Ther. 6:212.
3 Khosla S, Burr D, Cauley J, Dempster DW, Ebeling PR, Felsenberg D, Gagel RF, Gilsanz V,
4 Guise T, Koka S, et al. 2007. Bisphosphonate-associated osteonecrosis of the jaw:
5 report of a task force of the American Society for Bone and Mineral Research. J Bone
6 Miner Res. 22(10):1479-1491.
7 Khurana S, Verfaillie CM. 2013. Periostin acts as an important cell cycle regulator of adult
8 hematopoietic stem cells via binding to integrin-αvβ3. Blood.122(21):341.
9 Kikuiri T, Kim I, Yamaza T, Akiyama K, Zhang Q, Li Y, Chen C, Chen WJ, Wang S, Le AD,
10 Shi S. 2010. Cell-based immunotherapy with mesenchymal stem cells cures
11 bisphosphonate-related osteonecrosis of the jaw-like disease in mice. J Bone Miner
12 Res. 25(7):1668-1679.
13 Kim RH, Lee RS, Williams D, Bae S, Woo J, Lieberman M, Oh JE, Dong Q, Shin KH, Kang
14 MK, Park NH. 2011. Bisphosphonates induce senescence in normal human oral
15 keratinocytes. J Dent Res. 90(6):810-816.

Kordelas L, Rebmann V, Ludwig A-K, Radtke S, Ruesing J, Doeppner TR, Epple M, Horn PA, Beelen DW, Giebel B. 2014. MSC-derived exosomes: a novel tool to treat therapy-refractory graft-versus-host disease. Leukemia. 28(4):970-973

Lai RC, Chen TS, Lim SK. 2011. Mesenchymal stem cell exosomes: a novel stem cell-based therapy for cardiovascular disease. Regen Med. 6(4):481-492

Li Y, Xu J, Mao L, Liu Y, Gao R, Zheng Z, Chen W, Le A, Shi S, Wang S. 2013. Allogeneic mesenchymal stem cell therapy for bisphosphonate-related jaw osteonecrosis in swine. Stem Cells Dev. 22(14):2047-2056.

Liao Z, Luo R, Li G, Song Y, Zhan S, Zhao K, Hua W, Zhang Y, Wu X, Yang C. 2019. Exosomes from mesenchymal stem cells modulate endoplasmic reticulum stress to protect against nucleus pulposus cell death and ameliorate intervertebral disc degeneration in vivo. Theranostics. 9(14):4084-4100.

Liu J, Cao L, Chen J, Song S, Lee IH, Quijano C, Liu H, Keyvanfar K, Chen H, Cao LY, et al. 2009. Bmi1 regulates mitochondrial function and the DNA damage response pathway. Nature. 459(7245):387-392.

Matsubara K, Matsushita Y, Sakai K, Kano F, Kondo M, Noda M, Hashimoto N, Imagama S, Ishiguro N, Suzumura A, et al. 2015. Secreted ectodomain of sialic acid-binding Ig-like

lectin-9 and monocyte chemoattractant protein-1 synergistically regenerate transected rat peripheral nerves by altering macrophage polarity. J Neurosci. 35(6):2452-2464.

Mummery CL, Davis RP, Krieger JE. 2010. Challenges in using stem cells for cardiac repair. Sci Transl Med. 2(27):27ps17

Ogata K, Katagiri W, Osugi M, Kawai T, Sugimura Y, Hibi H, Nakamura S, Ueda M. 2015. Evaluation of the therapeutic effects of conditioned media from mesenchymal stem cells in a rat bisphosphonate-related osteonecrosis of the jaw-like model. Bone. 74:95-105.

Osugi M, Katagiri W, Yoshimi R, Inukai T, Hibi H, Ueda M. 2012. Conditioned media from mesenchymal stem cells enhanced bone regeneration in rat calvarial bone defects. Tissue Eng. 18(13-14):1479-1489.

Phinney DG, Pittenger MF. 2008. Concise review : MSC-derived exosomes for cell-free therapy. Stem Cells. 35(4):851-858.

Plotkin LI, Manolagas SC, Bellido T. 2006. Dissociation of the pro-apoptotic effects of bisphosphonates on osteoclasts from their anti-apoptotic effects on osteoblasts/osteocytes with novel analogs. Bone. 39(3):443-452.

Raposo G, Stoorvogel W. 2013. Extracellular vesicles: exosomes, microvesicles, and friends. J Cell Biol. 200(4):373-383.

Rodier F, Campisi J. 2011. Four faces of cellular senescence. J Cell Biol. 192(4):547-556.

Ruggiero SL, Dodson TB, Fantasia J, Goodday R, Aghaloo T, Mehrotra B, O'Ryan F. 2014. American association of oral and maxillofacial surgeons position paper on medication-related osteonecrosis of the jaw - 2014 update. J Oral Maxillofac Surg. 72(10):1938-1956.

Russell RGG, Watts NB, Ebetino FH, Rogers MJ. 2008. Mechanisms of action of bisphosphonates: similarities and differences and their potential influence on clinical efficacy. Osteoporos Int. 19(6):733-759.

Sonis ST, Watkins BA, Lyng GD, Lerman MA, Anderson KC. 2009. Bony changes in the jaws of rats treated with zoledronic acid and dexamethasone before dental extractions mimic bisphosphonate-related osteonecrosis in cancer patients. Oral Oncol. 45(2):164-172.

Théry C, Witwer KW, Aikawa E, Alcaraz MJ, Anderson JD, Andriantsitohaina R, Antoniou A, Arab T, Archer F, Atkin-Smith GK, et al. 2018. Minimal information for studies of extracellular vesicles 2018 (MISEV2018): a position statement of the International

Society for Extracellular Vesicles and update of the MISEV2014 guidelines. J Extracell Vesicles. 7(1):1535750.

Uccelli A, Moretta L, Pistoia V. 2008. Mesenchymal stem cells in health and disease. Nat Rev Immunol. 8(9):726-736.

Urbanowitz G, Yanagihara R, Zheng M, Gordon D, Rosen LS, Hirsh V, Krzakowski M, Pawlicki M, de Souza P, Tchekmedyian S, et al. 2003. Zoledronic acid versus placebo in the treatment of skeletal metastases in patients with lung cancer and other solid tumors: a phase III, double-blind, randomized trial--the zoledronic acid lung cancer and other solid tumors study group. J Clin Oncol. 21(16):3150-3157.

Valadi H, Ekström K, Bossios A, Sjöstrand M, Lee JL and Lötvall JO. 2007. Exosome-mediated transfer of mRNAs and microRNAs is a novel mechanism of genetic exchange between cells. Nat Cell Biol. 9(6):654-659.

Yamazaki H, Mori T, Yazawa M, Maeshima AM, Matsumoto F, Yoshimoto S, Ota Y, Kaneko A, Tsuda H, Kanai Y. 2013. Stem cell self-renewal factors Bmi1 and HMGA2 in head and neck squamous cell carcinoma: clues for diagnosis. Lab Investig. 93(12):1331-1338.

Yokoi A, Yoshioka Y, Yamamoto Y, Ishikawa M, Ikeda S, Kato T, Kiyono T, Takeshita F, Kajiyama H, Kikkawa F, et al. 2017. Malignant extracellular vesicles carrying MMP1 mRNA facilitate peritoneal dissemination in ovarian cancer. Nat Commun. 8:14470.

Zhang L, Chan C. 2010. Isolation and enrichment of rat mesenchymal stem cells (MSCs) and separation of single-colony derived MSCs. J Vis Exp. (37):1852.

Figure Legends

Figure 1. Characterization of MSC-derived EVs.

(A) Representative image of purified EVs obtained with transmission electron microscopy. They showed a spherical shape; scale bar 100 nm. (B) The particle size distribution of MSC-EVs using a particle size measurement system (ELSZ-2). The EVs collected by enrichment with PBS were 50 to 150 nm in diameter. (C) Western blot analysis of specific exosomal markers, CD63, CD9, and CD81. α-tubulin showed cellular components as a control. (D) Uptake analysis of MSC-EVs by rat bone marrow cells. PKH26 was labeled with red fluorescence, and the nuclei were stained with Hoechst33342; scale bar 50 μm.

Figure 2. Injection of MSC-EVs into rat BRONJ model.

(A) Development of rat BRONJ model and schedule of EVs injection. i.v., intravenous; s.i., subcutaneous injection. (B) Upper jaw specimens 2 and 8 weeks after tooth extraction. Black arrows indicate the tooth extracted parts. Wound healing was observed in the control and ZOL + EVs groups, but the wound was open in the ZOL + PBS group. (C) 3D-reconstructed μCT image of the maxilla and typical coronal cross-sectional image, two weeks after tooth extraction. White arrows indicate the extracted parts. (D) Evaluation of upper jaw 2 and 8 weeks after tooth extraction by H&E staining. Enlarged images of the tooth extracted parts, indicated by black arrows. The continuity of the epithelium was confirmed in control and the EVs injection group by H&E staining; scale bar 1 mm. (E) The graph shows the degree of wound closure at 3, 7, and 14 days. n = 3 per group in 3 and 7 days. n = 6 per group in 14 days. *p = 0.014 and *p = 0.02. (F) After 7 and 14 days, for each socket, a minimum cylinder containing the socket was set up and the percentage of bone volume was measured and summed. Bone mass/total tissue mass (%) according to the analysis software (CTAn). In the ZOL + PBS group, the volume of the bone including the socket was decreased compared

with that in the control group (*p < 0.001), and it was increased in the ZOL + EVs group, (*p < 0.001, *p = 0.002).

Figure 3. Administration of MSC-EVs to bone marrow cells and fibroblasts treated with 100 μM ZOL.

(A) β-galactosidase-positive cells (green) were observed by fluorescent immunostaining; scale bar 100 μm. Blue indicates DAPI; 4', 6-diamidino-2-phenylindole. (B, C) The time course of the number of β-galactosidase-positive cells of bone marrow cells and fibroblasts was shown in the graph. The administration of ZOL significantly increased the number of β-galactosidase-positive cells (both; *p < 0.001), while it was significantly reduced in the ZOL + EVs group (both; *p < 0.001). (D) Gene expression 48 hours after administration of EVs. The expression levels of *p21* and *pRB* involved in cellular senescence, and *IL-6*, *IL-8*, *MMP1,* and *MMP3*, which are SASP secreted by senescent cells, were upregulated in the ZOL + PBS group (all; *p < 0.001) but downregulated in the ZOL + EVs group (only *p21*; *p = 0.002, and the rest; *p < 0.001). (E) Migratory capacity of bone marrow cells and fibroblasts was assessed by wound healing assay. Images were taken at 48 hours after administration of EVs; scale bar 500 μm. (F) The graph shows the percentage of the scratch area closed 48

hours after the EVs administration. The scratched area was not reduced in the ZOL + PBS group compared with the control group (bone marrow cells; *p = 0.013, fibroblasts; *p < 0.001), but it was reduced in the ZOL + EVs group (bone marrow cells; *p = 0.005 and fibroblasts; *p < 0.002). (G) Cell viability was evaluated by WST-8. Although the ZOL + PBS group experienced a significant reduction in cell proliferation (bone marrow cells; *p < 0.001 and fibroblasts; *p = 0.001); compared to the control group, addition of EVs resulted in their restoration (bone marrow cells; *p < 0.001 and fibroblasts; *p = 0.002). n = 6 per group.

Figure 4. ZOL and MSC-EVs targets in rat models.

(A) Duplicated signals of the MSCs marker CD90 and the senescence marker β-galactosidase were observed only in the ZOL + PBS group in the extraction cavity; scale bar 50 μm. (B) The expression of periostin, which is expressed in osteoblasts, and the expression of β-galactosidase were confirmed by double staining. They overlapped only in the ZOL + PBS group, scale bar 50 μm. (C, D) Angiogenesis in tissues was assessed by immunofluorostaining of VEGFR2 and CD31. Although little expression was observed in the ZOL + PBS group, a strong green signal of VEGFR2 and CD31 was observed in the ZOL + EVs and the control groups; scale bar = 100 μm (C), 50 μm (D). (E) The number of

β-galactosidase-positive cells in the tooth extraction socket, as shown in the graph (n = 6 per group, three images per sample) (*p < 0.001). (F) The gene expression in rat maxillary bone tissue was evaluated at 14 days. The expression levels of *p21* and *pRB*, involved in cellular senescence, and *IL-6*, *IL-8*, *MMP1,* and *MMP3*, which are SASP secreted by senescent cells, were upregulated in the ZOL + PBS group (*p21, IL-6, IL-8,* and *MMP3*; *p < 0.001, *pRB*; *p = 0.001, *MMP1*; *p = 0.008) but downregulated in the ZOL + EVs group (*p21, IL-6, IL-8,* and *MMP3*; *p < 0.001, *pRB*; *p = 0.007, *MMP1*; *p = 0.017). *VEGF* expression levels were elevated in the ZOL + EVs groups (*p < 0.001). (G) Gene expression of *Bmi1* and *Hgma2* involved in stem cell self-renewal was elevated in the ZOL + EVs group (*Bmi1*; *p < 0.001 and *Hmga2*; *p = 0.004). n = 6 per group.

Figure 5. Effects of EVs on osteoclasts and cancer cells.

(A) *In vitro*, rat osteoclasts were cultured in ZOL, and their apoptosis was demonstrated by TUNEL staining; scale bar 100 μm. (B) Percentage of apoptotic osteoclasts. There were no apoptotic osteoclasts in the control group (p = 0.643) (n = 6 per group, 3 images per sample). Osteoclasts exhibited apoptosis upon administration of ZOL, as is the general effect of ZOL, and administration of EVs did not affect osteoclast viability. (C) *In vivo*, osteoclasts were

stained with TRAP. Although there were fewer osteoclasts stained in the ZOL + PBS and ZOL + EVs group than in the control group, the presence was confirmed, scale bar 500 μm. n = 6 per group. (D) As a result of administering ZOL and EVs to cancer cells, no obvious proliferation of cancer cells was observed (p = 0.766); n = 6 per group. (E) ZOL also acts on osteoblasts, stem cells, and fibroblasts, causing aging. These senescent cells secrete a different cytokine called SASP that cause chronic inflammation in the surrounding cells. In this cycle, MSC-EVs prevent the expression of *p21* and *pRB* in the senescence induction pathway, thereby preventing migration, inhibition of proliferation, and the subsequent adverse effects of senescent cells on the environment.

Figure 1.

Junna Watanabe et al.

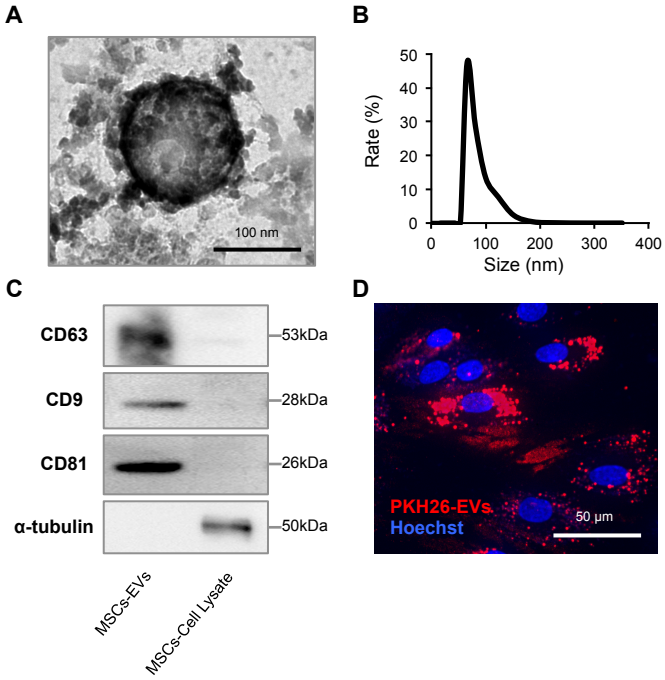

Figure 2.

Junna Watanabe et al.

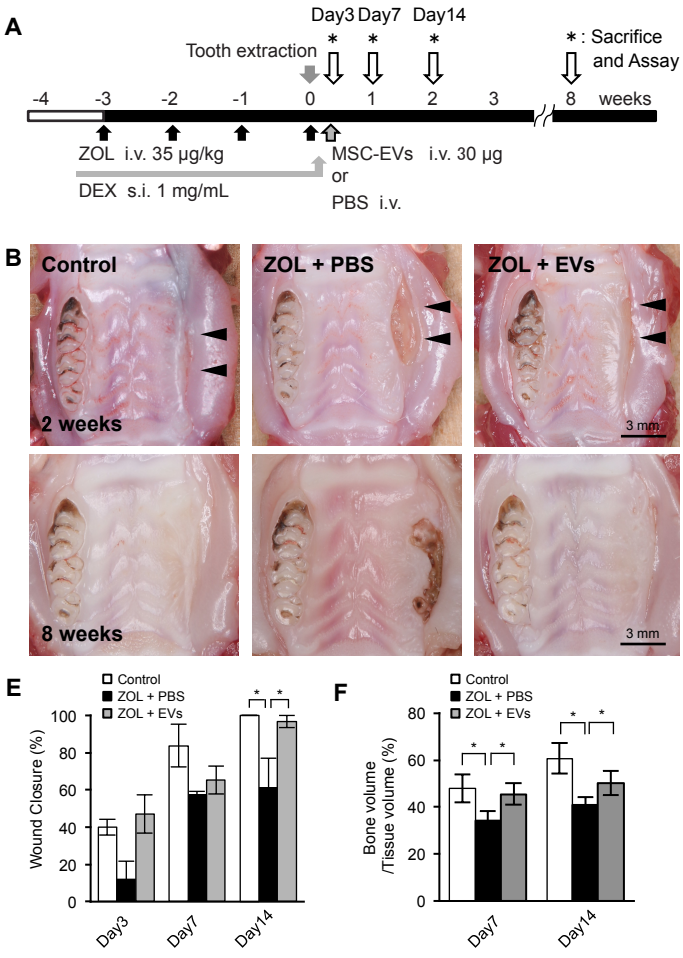

Figure 3.

Junna Watanabe et al.

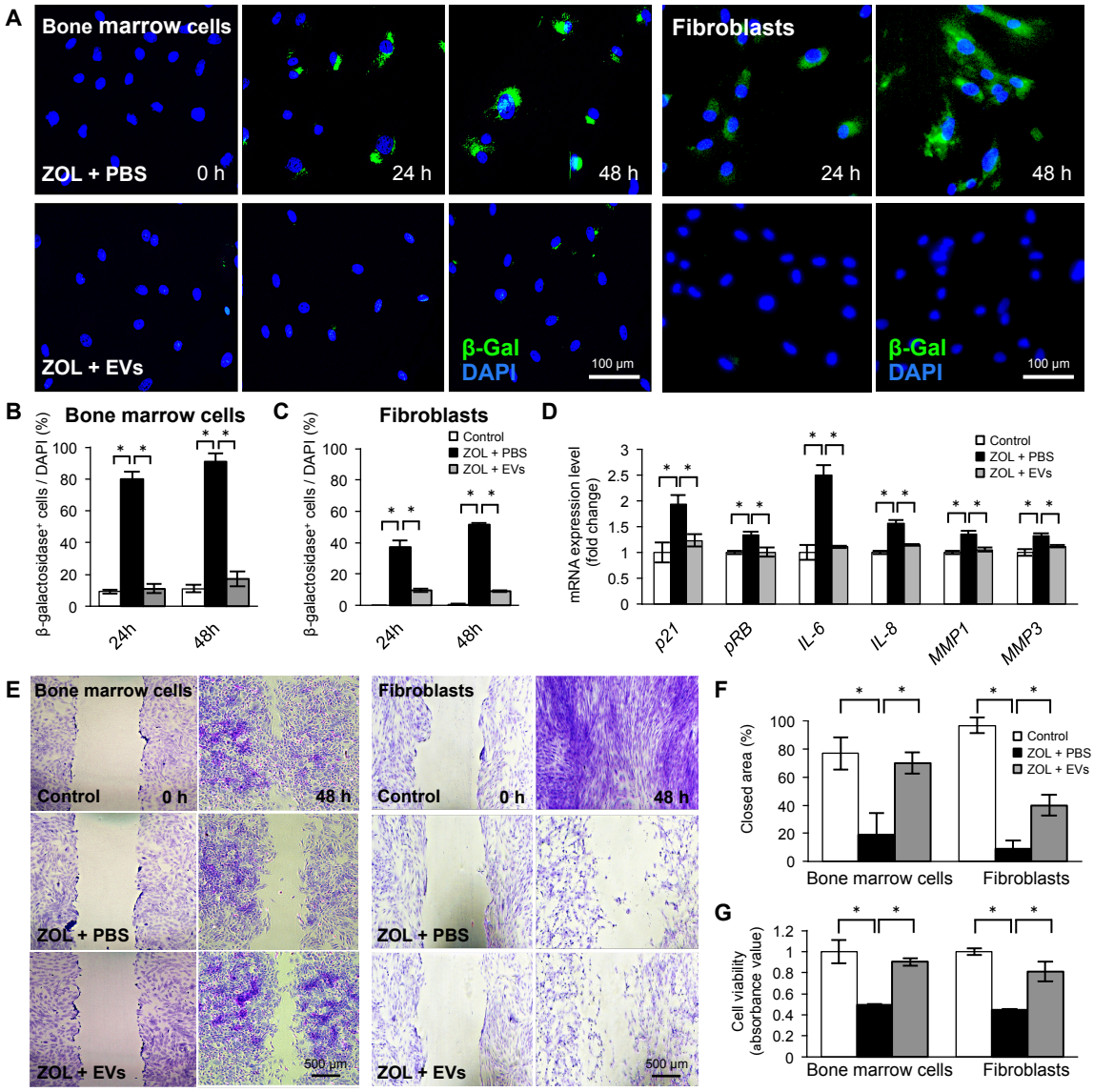

Figure 4.

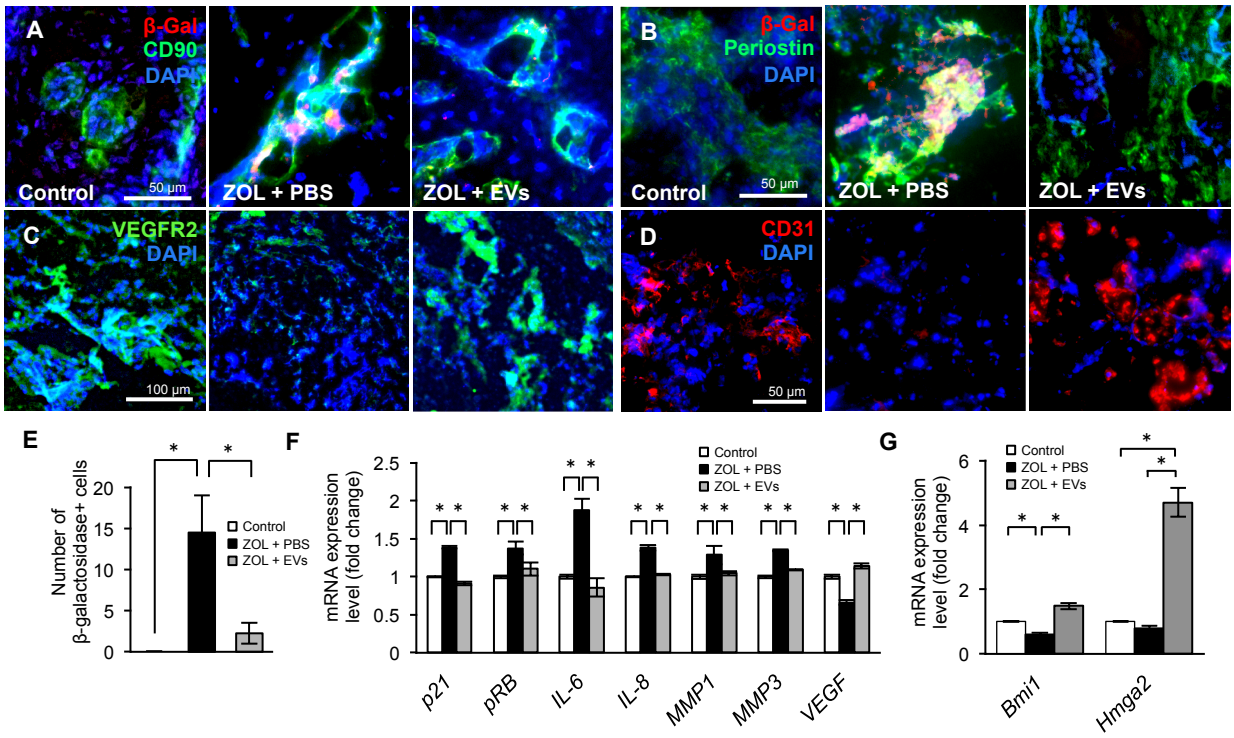
A
β-Gal
CD90
DAPI
Control
50 μm
ZOL + PBS
ZOL + EVs
B
β-Gal
Periostin
DAPI
Control
50 μm
ZOL + PBS
ZOL + EVs
C
VEGFR2
DAPI
100 μm
D
CD31
DAPI
50 μm
E
Number of β-galactosidase+ cells
Control
ZOL + PBS
ZOL + EVs
F
mRNA expression level (fold change)
Control
ZOL + PBS
ZOL + EVs
p21
pRB
IL-6
IL-8
MMP1
MMP3
VEGF
G
mRNA expression level (fold change)
Control
ZOL + PBS
ZOL + EVs
Bmi1
Hmga2

Figure 5.

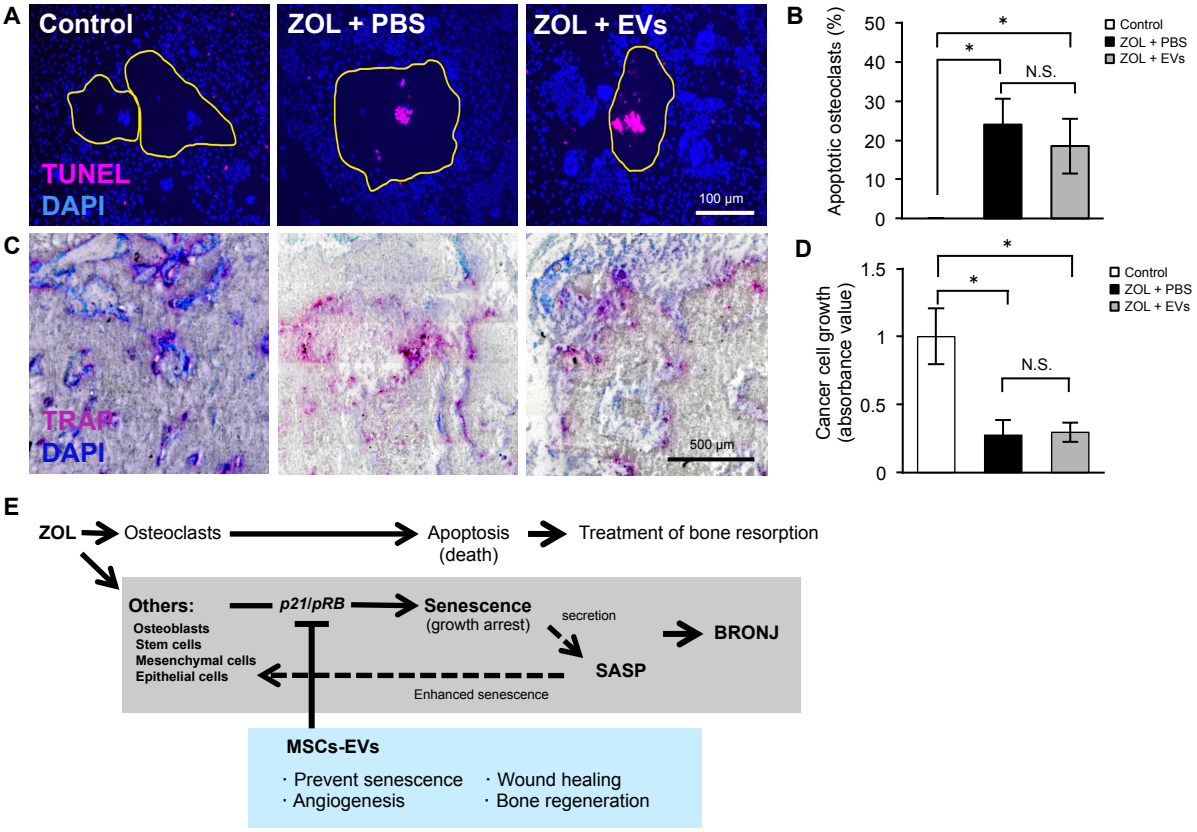
A
Control
ZOL + PBS
ZOL + EVs
TUNEL
DAPI
100 μm
B
Apoptotic osteoclasts (%)
50
40
30
20
10
0
*
*
N.S.
Control
ZOL + PBS
ZOL + EVs
C
TRAP
DAPI
500 μm
D
Cancer cell growth (absorbance value)
1.5
1
0.5
0
*
*
N.S.
Control
ZOL + PBS
ZOL + EVs
E
ZOL
Osteoclasts
Apoptosis (death)
Treatment of bone resorption
Others:
Osteoblasts
Stem cells
Mesenchymal cells
Epithelial cells
p21/pRB
Senescence (growth arrest)
secretion
SASP
BRONJ
Enhanced senescence
MSCs-EVs
· Prevent senescence
· Angiogenesis
· Wound healing
· Bone regeneration

Appendix Figure 1.

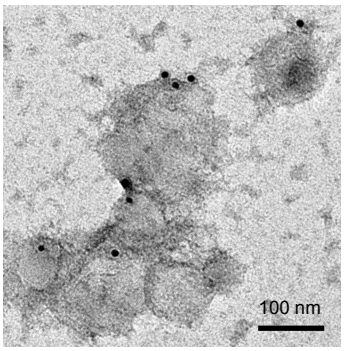

Appendix Figure 2.

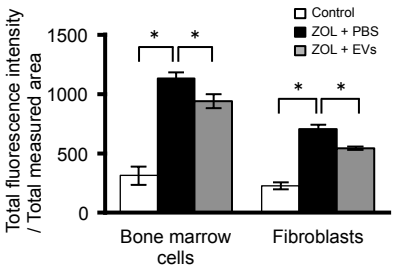

Appendix Figure 3.

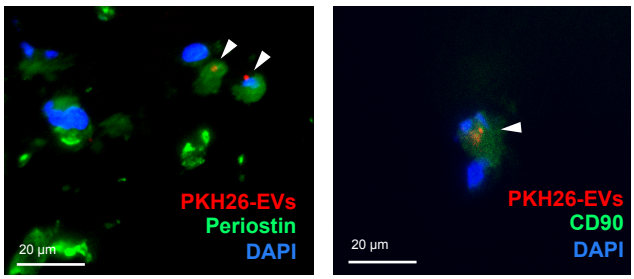

Appendix Figure 4.

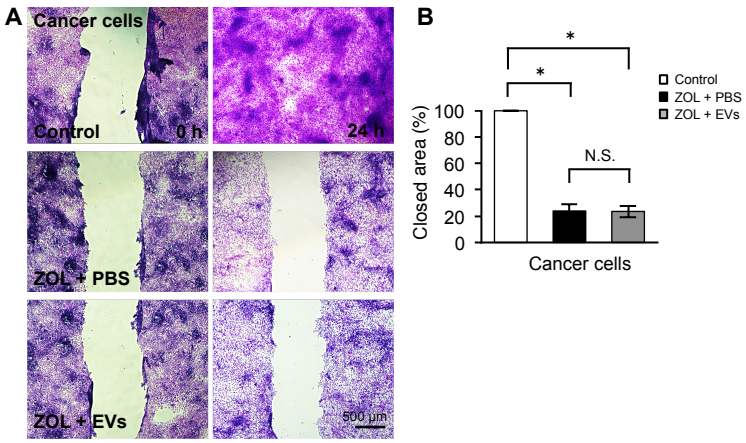

Appendix Table. Primer sequences used in qRT-PCR

Primer	Sequence (forward 5'-3')	Sequence (reverse 5'-3')
GAPDH	AACTTTGGCATCGTGGAAGG	CGGATACATTGGGGGTAGGA
p21	AGTAGACACGAAACAGGCTCAG	TCAACACCCTGTCTTGTCTTCG
pRB	GCATCGAATCATGGAATCCCTTGC	GAGGGAGGCTGAGAGAACAAGC
IL-6	TTCTGTCTCGAGCCCACCAG	GGAAGGCAGTGGCTGTCAAC
IL-8	CATTAATATTTAACGATGTGGATGCGTTTCA	GCCTACCATCTTTAAACTGCACAAT
MMP1	GCCCGGCAGAATGTGGAAAC	TCACCTCCTTGGCATCCACG
MMP3	TGAACTTGGCCACTCCCTGG	AGAGATGGAAACGGGCCAGG
VEGF	ACCAAAGCCAGCACATAGGA	GGGGCATTAACTGCATCTGG
Bmi1	ATGCAGCTCACCCTTCAGCA	CGACCTGCTTGGGTGGAAGA
Hmga2	CCACATCAGCCCAGGGACAA	GGGCTCTTGTTCTTGCTGCC

Appendix Data.

Figure 2.

E **Wound closure (%)**

	control	ZOL+PBS	ZOL+EVs	*p* value a	b	c
Day3	39.92 ± 3.47	12.2 ± 9.46	47.05 ± 10.22	$p = 0.325$	$p = 0.116$	$p = 0.999$
Day7	83.68 ± 7.59	57.83 ± 11.39	65.27 ± 1.48	$p = 0.408$	$p = 0.999$	$p = 0.786$
Day14	100 ± 0.00	61.6 ± 15.55	96.67 ± 3.2	$^*p = 0.014$	$^*p = 0.02$	$p = 0.931$

F **Bone volume/Tissue volume (%)**

	control	ZOL+PBS	ZOL+EVs	a	b	c
Day7	47.80 ± 5.95	34.34 ± 3.80	45.52 ± 4.50	$^*p < 0.001$	$^*p < 0.001$	$p = 0.584$
Day14	60.71 ± 6.61	40.90 ± 3.44	50.33 ± 5.22	$^*p < 0.001$	$^*p = 0.002$	$^*p = 0.001$

Figure 3.

B **β-galactosidase+ cells/DAPI (%)**

Bone marrow cells	control	ZOL+PBS	ZOL+EVs	a	b	c
24h	9.09 ± 1.15	80 ± 4.61	11.11 ± 2.98	$^*p < 0.001$	$^*p < 0.001$	$p = 0.61$
48h	11.11 ± 2.58	90.6 ± 35.53	17.14 ± 4.62	$^*p < 0.001$	$^*p < 0.001$	$p = 0.671$

C **β-galactosidase+ cells/DAPI (%)**

Fibroblasts	control	ZOL+PBS	ZOL+EVs	a	b	c
24h	0 ± 0.00	37.10 ± 4.62	9.43 ± 1.15	$^*p = 0.002$	$^*p = 0.012$	$p = 0.289$
48h	0.56 ± 0.57	51.3 ± 51.52	8.93 ± 0.58	$^*p = 0.001$	$^*p = 0.021$	$p = 0.802$

D **mRNA expression level (fold change)**

	control	ZOL+PBS	ZOL+EVs	a	b	c
p21	1 ± 0.19	1.94 ± 0.17	1.24 ± 0.12	$^*p < 0.001$	$^*p = 0.002$	$p = 0.132$
pRB	1 ± 0.04	1.34 ± 0.06	1.00 ± 0.09	$^*p < 0.001$	$^*p < 0.001$	$p = 0.647$
IL-6	1 ± 0.14	2.51 ± 0.19	1.11 ± 0.02	$^*p < 0.001$	$^*p < 0.001$	$p = 0.49$
IL-8	1 ± 0.03	1.57 ± 0.07	1.15 ± 0.01	$^*p < 0.001$	$^*p < 0.001$	$^*p < 0.001$
MMP1	1 ± 0.03	1.36 ± 0.06	1.06 ± 0.04	$^*p < 0.001$	$^*p < 0.001$	$p = 0.2$
MMP3	1 ± 0.07	1.32 ± 0.06	1.12 ± 0.02	$^*p < 0.001$	$^*p < 0.001$	$^*p < 0.001$

E **Closed area (%)**

	control	ZOL+PBS	ZOL+EVs	a	b	c
Bone marrow cells	76.93 ± 11.49	19.08 ± 15.59	70.09 ± 7.51	$^*p = 0.003$	$^*p = 0.005$	$p = 0.773$
Fibroblasts	96.93 ± 5.49	9.08 ± 5.59	40.09 ± 7.51	$^*p = 0.001$	$^*p = 0.002$	$^*p = 0.003$

F **Cell viabillity (absorbance value)**

	control	ZOL+PBS	ZOL+EVs	a	b	c
Bone marrow cells	1 ± 0.11	0.49 ± 0.01	0.90 ± 0.03	$^*p < 0.001$	$^*p < 0.001$	$p = 0.145$
Fibroblasts	1 ± 0.03	0.44 ± 0.01	0.81 ± 0.10	$^*p = 0.001$	$^*p = 0.002$	p = 0.527

Figure 4.

E **Number of β-galactosidase+ cells**

control	ZOL+PBS	ZOL+EVs	a	b	c
0 ± 0.00	15 ± 3.56	2.25 ± 1.26	$^*p < 0.001$	$^*p < 0.001$	$p = 0.353$

F **mRNA expression level (fold change)**

	control	ZOL+PBS	ZOL+EVs	a	b	c
p21	1 ± 0.01	1.38 ± 0.01	0.91 ± 0.03	$^*p < 0.001$	$^*p < 0.001$	$p = 0.993$
pRB	1 ± 0.02	1.38 ± 0.08	1.10 ± 0.09	$^*p = 0.001$	$^*p = 0.007$	$p = 0.25$
IL-6	1 ± 0.02	1.89 ± 0.15	0.86 ± 0.12	$^*p < 0.001$	$^*p < 0.001$	$p = 0.335$
IL-8	1 ± 0.01	1.38 ± 0.04	1.03 ± 0.01	$^*p < 0.001$	$^*p < 0.001$	$p = 0.27$
MMP1	1 ± 0.03	1.29 ± 0.13	1.05 ± 0.03	$^*p = 0.008$	$^*p = 0.017$	$p = 0.731$
MMP3	1 ± 0.02	1.35 ± 0.01	1.09 ± 0.01	$^*p < 0.001$	$^*p < 0.001$	$^*p < 0.001$
VEGF	1 ± 0.03	0.66 ± 0.03	1.14 ± 0.03	$^*p < 0.001$	$^*p < 0.001$	$^*p < 0.001$

G **mRNA expression level (fold change)**

	control	ZOL+PBS	ZOL+EVs	a	b	c
Bmi1	1 ± 0.01	0.61 ± 0.05	1.48 ± 0.10	$^*p = 0.001$	$^*p < 0.001$	$^*p < 0.001$
Hmga2	1 ± 0.01	0.76 ± 0.10	1.41 ± 1.46	$p = 0.956$	$^*p = 0.004$	$^*p = 0.005$

Figure 5.

B **Apoptotic osteoclasts (%)**

control	ZOL+PBS	ZOL+EVs	a	b	c
0 ± 0.00	24 ± 6.70	18.52 ± 7.03	$^*p = 0.006$	$p = 0.643$	$^*p = 0.015$

D **Cancer cell grouth (absorbance value)**

control	ZOL+PBS	ZOL+EVs	a	b	c
1 ± 0.21	0.28 ± 0.11	0.30 ± 0.07	$^*p < 0.001$	$p = 0.766$	$^*p < 0.001$

Appendix Figure 2.

	control	ZOL+PBS	ZOL+EVs	a	b	c
Bone marrow cells	311.76 ± 78.48	1126.84 ± 56.27	938.55 ± 60.39	$^*p < 0.001$	$^*p = 0.029$	$^*p < 0.001$
Fibroblasts	225.37 ± 31.13	707.15 ± 33.93	543.63 ± 15.32	$^*p < 0.001$	$^*p = 0.027$	$^*p < 0.001$

Appendix Figure 4.

B **Closed area (%)**

	control	ZOL+PBS	ZOL+EVs	a	b	c
Cancer cells	100.00 ± 0	23.92 ± 4.86	23.58 ± 4.40	$^*p < 0.001$	$p = 0.993$	$^*p < 0.001$

Extracellular vesicles of stem cells to prevent BRONJ

Junna Watanabe, Kiyoshi Sakai, Yusuke Urata, Naoto Toyama, Eiji Nakamichi, Hideharu Hibi

Department of Oral and Maxillofacial Surgery, Nagoya University Graduate School of Medicine, Nagoya, Japan

Appendix Materials and Methods

General Anesthesia and Local Anesthesia

The rats were first sedated by inhalation of 2% isoflurane. The three mixed anesthetics were anesthetized by intraperitoneal injection of 0.1 mL per 10 g body weight. The composition was diluted with physiological saline so that medetomidine hydrochloride (Kyoritsu Seiyaku Corporation, Tokyo, Japan) 0.15 mg / kg + midazolam (Astellas Pharma Inc, Tokyo, Japan) 2 mg / kg + butorphanol tartrate (Meiji Seika Pharma Co., Ltd., Tokyo, Japan) 2.5 mg / kg (Flecknell 2009). Supplemental local anesthesia was given to the rats as needed by local infiltration, with a few drops of 2% lidocaine containing 1:100,000 epinephrine (ORA Inj. Dental Cartridge, Tokyo, Japan) delivered into the mucobuccal fold.

Observation of EVs Using a Transmission Electron Microscope

For negative staining, 10μL of MSC-EVs was placed on a hydrophilic-treated 200-mesh carbon-coated grid (Nisshin EM Co., Ltd. Tokyo, Japan), washed with distilled water, and stained with 2% uranyl acetate dropwise. The excess liquid was sucked off with a filter paper, dried, and observed using a transmission electron microscope (JEM-1400PLUS, JEOL, Tokyo, Japan).

For immunogold staining, 10μL of MSC-EVs were loaded on the grid and blocked with 1% bovine serum albumin for 1 hour. The grid was placed on a drop containing diluted primary antibody (anti-CD9, 1:50, System Biosciences, Palo Alto, CA) for 1 hour at room temperature. After washing with PBS, the grid was treated with 10 nm gold-labeled secondary antibody (1:50, G7402, Sigma) for 1 hour at room temperature. After washing with PBS, the sample was fixed with 1% glutaraldehyde for 10 minutes. After washing with PBS and distilled water, the cells were stained with 1% Uranyl acetate, and the excess liquid was blotted with filter paper and dried. The sample was observed using JEM-1400PLUS.

Measurement of EVs Particle Size

To determine the particle size distribution of MSCs-EVs, this experiment was performed using a particle size measurement system (ELSZ-2, Otsuka Electronics Co., Ltd.), according to instructions. Since the particles in the solution perform Brown motion depending on the particle size, the particle size and distribution of that were determined by analyzing the scattered light obtained when the particles were irradiated with light.

Western Blot for EVs

To extract EVs proteins, 200 μL of RIPA buffer (Thermo Fisher Scientific) was added to recover the EVs pellets, and thermal denaturation was added and used for Western blot. Western blot confirmed the purification by detecting exosomal marker proteins rabbit anti-human CD63, CD9, and CD81 with goat anti-rabbit HRP secondary antibody (1:500, System Biosciences). As a control, anti-mouse α-tubulin (1:500, Ab-1, Merck Millipore) was used.

Histological Specimens (Paraffin-embedded and Frozen Specimens)

The tissues were decalcified with EDTA for 1 month, embedded in paraffin, sliced at 4 μm thickness, and stained with H&E staining.

The frozen sections were prepared using the Kawamoto method (Kawamoto 2003). The upper jaw was isolated and embedded in super cryo-embedding medium (SECTION-LAB Co. Ltd., Hiroshima, Japan), and 4 μm coronal sections were generated with a cryostat (CM3050S, Leica Biosystems). The sections were dried for 10 seconds, fixed with 100%

ethanol for 1 minute, and 4% PFA for 2 minutes. Next, sections underwent immunofluorescence or TRAP staining. For immunofluorescence staining, samples were blocked with 3% bovine serum albumin for 1 hour and incubated overnight with the following primary antibodies: anti-beta galactosidase (1:1000, ab9361, Abcam, Cambridge, UK), anti-CD90/Thy-1 (1:1000, ab225, Abcam), anti-Periostin (1:100, ab14041, Abcam), anti-VEGFR2 (1:100, ab39250, Abcam), and anti-CD31 (1:40, 550300, BD Pharmingen, Franklin Lakes, NJ). The following secondary antibodies were used: anti-chicken IgG Alexa Fluor 594 (1:1000, ab150172, abcam), anti-mouse IgG Alexa Fluor 488 (1:1000, ab150117, abcam), anti-mouse IgG Alexa Fluor 633(1:1000, A-21052, Thermo Fisher Scientific) and anti-rabbit IgG Alexa Fluor 488 (1:1000, A-21206, Thermo Fisher Scientific). After counterstaining with 4',6-diamidino-2-phenylindole (DAPI, NucBlue Fixed Cell ReadyProbes Reagent, Thermo Fisher Scientific), tissue images were observed through a universal fluorescence microscope (BZ9000; Keyence). For TRAP staining, the TRAP/ALP stain kit (FUJIFILM Wako Pure Chemical Corporation, Osaka, Japan) was used according to the manufacturer's instructions.

μCT Imaging

For observation with μCT, the tissues were quickly fixed in 4% paraformaldehyde and images taken using μCT (SkyScan 1176, Bruker, Billerica, MA) and using a 3D-reconstructed software program (NRecon and CTVox, Bruker). For each socket, a minimum cylinder containing the socket was set up, and the percentage of bone volume was measured (bone volume / total tissue volume (%)) (DataViewer64 and CTAn, Bruker). The imaging conditions and thresholds of μCT were kept constant across all analyses. Two blinded investigators performed all measurements.

Quantitative Real-time PCR (qRT-PCR)

The extracted tissues were removed and weighed to ensure consistency among groups, and RNA was extracted. Total RNA was isolated from the maxillary bone extraction site, which was flash-frozen in liquid nitrogen, and then crushed with Multibeads shocker (Yasui Kikai Corporation) and extracted with TRIzol reagent (Thermo Fisher Scientific), according to the manufacturer's protocol. A spectrophotometer was used to quantify total RNA levels, and RNA integrity was checked on 1% agarose gels. Reverse transcription reactions were performed with Superscript IV reverse transcriptase (Thermo Fisher Scientific) using 0.5 μg total RNA in a 20 μL total reaction volume. The quantitative real-time polymerase chain

reaction (qRT-PCR) was performed using THUNDERBIRD SYBR qPCR Mix (Toyobo, Osaka, Japan) and the Mx3005P QPCR System (Agilent Technologies, Tokyo, Japan). The specific primers were designed using Primer3 (Appendix Table: *p21*, *pRB*, *IL-6*, *IL-8*, *MMP1*, *MMP3*, *VEGF*, *Bmi1* and *Hgma2*). All results are normalized to *glyceraldehyde 3-phosphate dehydrogenase* (*GAPDH*). Gene expression fold changes were calculated relative to the control.

Quantification of Senescent Cells

Bone marrow cells and fibroblasts were cultured on CELLview Slides (Greiner Bio-One International GmbH, Kremsmünster, Austria). Each experimental group was created and scored by High Content Cell Imaging using Arrayscan VTI (Thermo Fisher Scientific). This technical approach quantified β-galactosidase-positive cells 24 hours after EVs administration. For High Content Cell Imaging, after immunostaining for β-galactosidase and DAPI, Arrayscan (Cellomics, ThemoFisher) was used to scan CELLview Slides at 10-fold magnification (n = 3 per group). Using the Cell Health Profiling application (Cellomics), recognition of the nuclear region and the FITC fluorescence intensity measurement area of the cytoplasm were set to a constant. Further, all wells were scanned with the same settings

for the largest area that could be measured for each well. The image was then analyzed using the software vHCS (Cellomics).

Tracking of PKH26-labeled EVs in the rat BRONJ model

The purified EVs were fluorescently labeled with PKH26 (Sigma-Aldrich; 4 μM) using Amicon Ultra-0.5mL centrifugal filter-100K (Merck Millipore), according to the manufacturer's instructions. For comparison, PBS was labeled with PKH26. PKH26-labeled EVs or PBS were injected into the tail vein of ZOL-treated rats created as described in the main manuscript (PKH26-labeled EVs; n = 5, PKH26-labeled PBS; n = 5). The rats were sacrificed on the day following treatment with PKH26-EVs. Frozen sections of the palate were prepared using the Kawamoto method as described above, and immunofluorostained with anti-Periostin (1:100, ab14041, Abcam), anti-CD90 (1:1000, ab225, Abcam) and DAPI. Tissue images were observed through a fluorescence microscope (BZ9000).

Appendix Reference

Flecknell P. 2009. Laboratory Animal Anaesthesia. 3rd ed. London. Elsevier.

Kawamoto T. 2003. Use of a new adhesive film for the preparation of multi-purpose fresh-frozen sections. Arch Histol Cytol.

Appendix Figure Legends

Apeendix Figure 1. Immunogold labeling for MSC-EVs

TEM image of MSC-EVs immunostained with anti-CD9 primary antibody, which is exosome marker, and 10 nm gold-labeled secondary antibody. The gold colloid adhered to the vesicles approximately 100 nm in size. When stained with the secondary antibody alone, no gold colloid was attached (Image not shown).

Apeendix Figure 2. Quantification of β-galactosidase positive cells

In each group, all cells in the well (4000 cells per group, n = 3) were counted. It shows a histogram of the fluorescence intensity and cell number of all cells measured in a representative well. The total fluorescence intensity of β-galactosidase was divided by the measured area for comparison. Compared with the control group, there was a significant increase in senescent cells in the ZOL + PBS group (bone marrow cells; $*p < 0.001$,

fibroblasts; *p < 0.001) and recovery in the ZOL + EVs group (bone marrow cells; *p = 0.029, fibroblasts; *p = 0.027).

Apeendix Figure 3. Tracking of PKH26-labeled EVs in the rat BRONJ model

PKH26-labeled EVs was observed in all treated rats (n = 5) as red dots in the socket tissue; scale bar 1 mm. It was not observed in the socket tissue of rats administered PKH26-labeled PBS (n = 5).

Apeendix Figure 4. Wound healing assay in cancer cells

The migratory capacity of cancer cells with ZOL was assessed by wound healing assay. Images were taken at 24 hours after administration of EVs; scale bar 500 μm. The graph shows the percentage of the scratch area closed 24 hours after the EVs administration. The scratched area was not reduced in both the ZOL + PBS group and the ZOL + EVs group compared with the control group (*p < 0.001).

Appendix Data.

Results are presented as mean ± SEM. *p* values are presented a; Control versus ZOL + PBS, b; ZOL + PBS versus ZOL + EVs and c; Contol versus ZOL + EVs.